

NON-INTRUSIVE DENSITY MEASUREMENTS IN A GRAVITY CURRENT OVER A POROUS BED

CLAUDIA ADDUCE⁽¹⁾, RUI FERREIRA⁽²⁾, GABRIEL SOLIS⁽¹⁾ & ANA MARGARIDA RICARDO⁽²⁾

⁽¹⁾ University Roma Tre, Rome, Italy
claudia.adduce@uniroma3.it

⁽²⁾ Instituto Superior Tecnico, Lisbon, Portugal
ruimferreira@ist.utl.pt

ABSTRACT

Gravity currents are buoyancy driven flows in which the density gradient causes the development of the flow predominantly in the horizontal direction. In this work, full depth lock-release gravity currents, propagating over a porous bed, are investigated by laboratory experiments. All experiments were recorded by a high-speed camera and an image analysis technique was applied for the evaluation of the instantaneous density fields of the surface gravity current and of the ground flow. The different steps of the non-intrusive density measurements, i.e. the gray scale calibration, the double calibration, the dynamic range and the image subtraction, are described and discussed. In particular, due to the large optical difference between the images captured for gravity currents and ground flow, a double calibration was adopted to analyze the two different flows. Preliminary results of the non-intrusive density measurements are shown. In the upper measurement domain, the instantaneous density fields show a gravity current with a well-defined head losing mass as it propagates downstream. In the bottom measurement domain, a second gravity current with an approximately triangular shape propagates slowly in the same direction of the surface current. In addition, infiltration, due to the presence of a top layer of salty water, develops a fingering instability.

Keywords: Image analysis technique; density evaluation; gravity currents; porous bed

1 INTRODUCTION

Gravity currents are flows driven by a horizontal density gradient between two fluids. The density difference between the current and the surrounding fluid can be due to temperature or salinity gradients, or to the presence of suspended particles, in which case the current is referred to as a turbidity current. Gravity currents play a key role in both natural and industrial flows as the spread of pollutant discharges in water bodies, oil spillages, oceanic overflows, sand storms and avalanches. Furthermore, gravity currents flowing over porous media are responsible for the flow of gas, water and petroleum within oil reservoirs during oil extraction and the long-term geological storage of carbon dioxide (CO₂) within underground saline aquifers.

Gravity currents propagating over an impermeable smooth bed have been widely investigated by both laboratory experiments (Hacker et al., 1996; Marino et al., 2005; Dai, 2013; Lombardi et al., 2018) and numerical simulations (Ooi et al., 2009; La Rocca et al., 2013; Dai 2016; Ottolenghi et al., 2017a; Inghilesi et al., 2018; Ottolenghi et al., 2018). While a few studies focused on gravity currents flowing over rough (Ozgekmen & Fischer, 2008; Nogueira et al., 2013; 2014; Bhaganagar, 2014; Ottolenghi et al., 2017b; Zordan et al., 2018) and rough-porous beds (Huppert & Woods, 1995; Woods & Mason, 2000; Golding et al., 2017) have been performed, further study is needed to understand how surface gravity currents transfer mass of a denser fluid to the porous medium and how ground flow gravity currents propagate.

To bridge this knowledge gap, a non-intrusive density measurement technique is developed and described in detail in the remainder of the paper. The technique is applied to measure the instantaneous density field in a gravity current flowing over and within a porous rough bed.

The paper is organized as follows: the experimental set-up and the laboratory experiments are illustrated in section 2, the non-intrusive density evaluation by image analysis is described in section 3, the experimental results are shown in section 4 and the conclusions are given in section 5.

2 EXPERIMENTAL SET-UP

Laboratory experiments were performed at the Hydraulics Laboratory of the Civil Engineering Department at Instituto Superior Técnico, using a glass tank 3 m long, 0.05 m wide and 0.4 m deep. The tank bottom was made of PVC (polyvinyl chloride). The tank was divided in two different volumes by a removable thin gate (with a height of 0.4 m, a width of 0.05 m and a thickness of 0.001 m), placed at a distance $x_0 = 0.2$ m from the left wall, see Figure 1. A PVC vertical barrier partitioned the main part of the channel, with $0 < x < 2.4$ m, from the

calibration section, positioned at the end of the tank, i.e. $2.4\text{ m} < x < 3\text{ m}$. A ruler, 3 m long, was positioned at bottom of the channel. Gravity currents were produced by the standard lock-release technique. Then the right part of the tank was filled with an ambient fluid at density ρ_2 , while the left part, i.e. the lock, was filled with salty water at density $\rho_1 > \rho_2$. Both volumes were filled up to the same height H , i.e. full-depth, lock-exchange experiments were performed. A controlled quantity of dye, Rhodamine, was added to the salty water in order to allow the visualization of the dense fluid (see Figure 2) and to evaluate the density field. For all the experiments both ρ_1 and ρ_2 were kept constant. In particular, the dense fluid was salty water with $\rho_1 = 1005.5\text{ Kg/m}^3$, while the ambient fluid was a solution of ethanol and water with a concentration of 4.4% ethanol by weight in solution (220 ml/5000 ml) and a density $\rho_2 = 990\text{ Kg/m}^3$.

Both in the right and the left part of the tank, a layer of translucent glass spheres, with a thickness $h_b = 0.1\text{ m}$ and a diameter of 0.003 m, was positioned on the bottom as porous bed. The unimodal porous bed was composed of 22 kg of beads. When the 0.003 m spheres were mixed, the density of the porous bed fluctuated between 0.6 and 0.637. This is true for random loose packing. Experiments were also performed first with no porous bed, i.e. gravity currents flowing over a smooth horizontal impermeable bed, in order to have base cases and then repeated with porous beds. The initial water depth in the tank h_0 was kept constant and $h_0 = 0.1\text{ m}$.

The experiment begins when the sliding gate is removed and the heavier fluid collapses starting to flow along the channel and creating a gravity current. While the surface gravity current flow propagates, an inspection of the bed underneath reveals the formation of the fingers associated to the infiltration of the denser fluid in the pores initially occupied by the lighter ambient fluid. In addition, in the left part of the tank, a salty current begins to flow within the porous media in the same direction of the surface gravity current, but with a lower velocity and with a sharp front shape.

Each experiment was recorded by an Allied Vision Bonito CL-400B/C high-speed camera with a frequency of 386 Hz and a resolution of 2320 x 1726 pixels. A back light panel 0.3 m high and 0.61 m long, i.e. a LED panel, was used for the illumination of the experiments. The panel was located behind the thin sheet of glass cross-sectioning the length of the tank. Each experiment was repeated in order to allow to record two different areas, i.e. the areas shown by the dashed lines in Figure 1, positioned at $0.20\text{ m} < x < 0.54\text{ m}$ and $0.62\text{ m} < x < 1.02\text{ m}$, respectively. Then, in the first area the behavior of the dense fluid once the lock has been released could be observed, while the second area started 0.42 m downstream the lock. StreamPix 5, developed by NorPix, was used as camera recording software. A 0.4 m x 0.175 m transparent checkerboard was used to correct the distortion of the camera. It was placed inside the channel and moved at different angles to allow the evaluation of the camera distortion. A pycnometer with a volume of 100 ml was used together with a digital balance (with an accuracy of $\pm 0.002\text{ g}$) for measuring the density of the fluids. In order to increase the accuracy of the measured quantities, for each experimental condition, i.e. initial water depth and bed composition, the experiment was repeated three times.

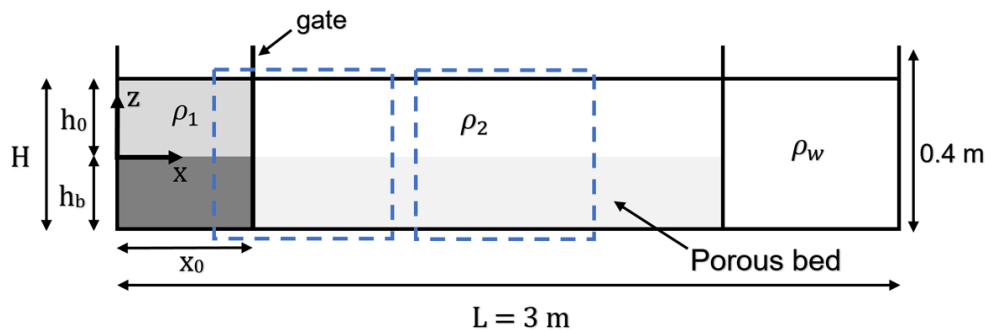


Figure 1. Sketch of the tank used to perform laboratory experiments

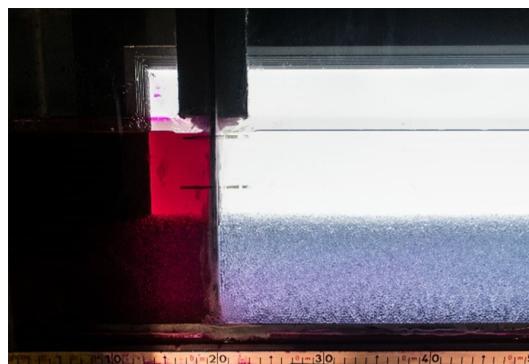


Figure 2. Initial condition for an experiment with a porous bed at the first measurement area

3 NON-INTRUSIVE DENSITY EVALUATION BY IMAGE ANALYSIS

3.1 Gray scale calibration

The definition of the image intensity range is important for a correct evaluation of the density in each pixel. The camera operates in a greyscale range, which is affected by the Rhodamine concentration, the aperture of the lens and the exposure time. The ideal greyscale range would vary between 0 (darkest shade of black) and 255 (lightest shade of white), although it is not possible due to two main reasons. First, even though a large quantity of Rhodamine could be added to water, it is not possible to reach the darkest gray scale because the colorant is red. Second, it is necessary to apply the shade of white, representing the ambient fluid, at a value lower than 255 in order to establish a dynamic range. If the value would be set at the upper limit of 255, it would not be possible to change the value, even if the color becomes brighter.

Thus, in order to establish the optimal range, an initial calibration experiment was conducted, following 9 steps, by adding Rhodamine to reach the lowest greyscale value as possible, i.e. the darkest shade of black. Initially, a small portion of the channel was filled with water and the brightness of the camera was set to get the first white color value slightly below 255. Afterwards, small quantities of Rhodamine were progressively added. Figure 3 shows the darkening of the water due to an increase in Rhodamine concentration.

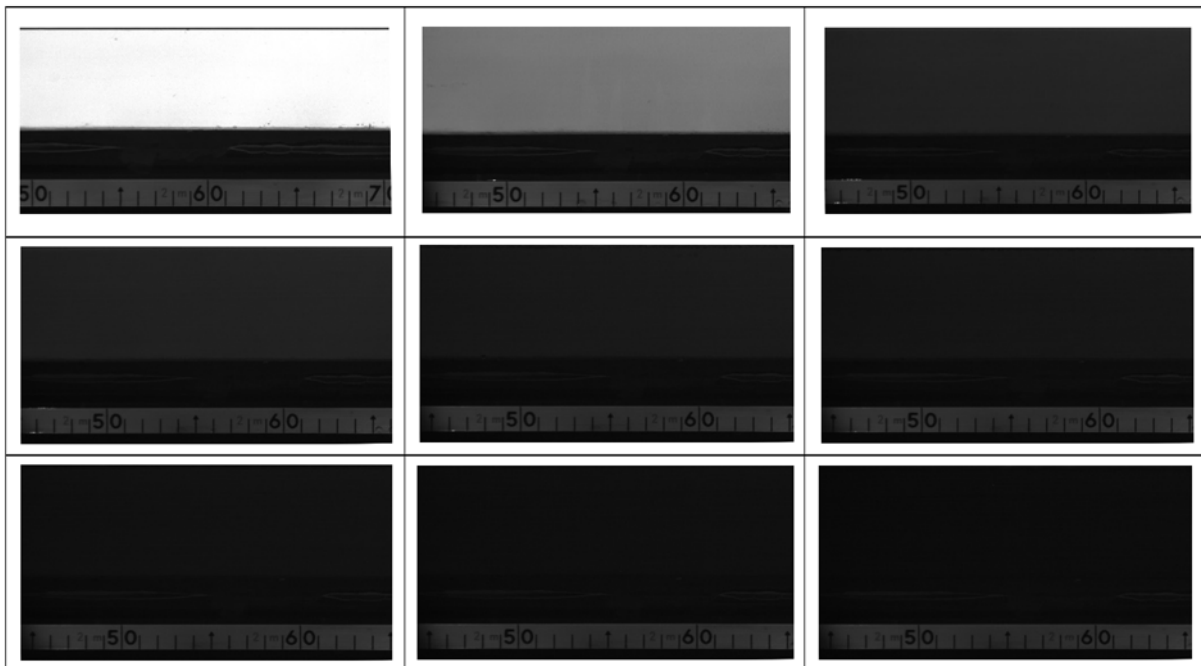


Figure 3. Gradual darkening of frames due to the increase in Rhodamine concentration

As shown in Figure 4, it was possible to obtain a color range between 50 and 251. In order to reach a very dark gray scale, i.e. a low RGB value of 17, it was necessary to use a large quantity of Rhodamine, which is not convenient since the Rhodamine is expensive. Then a dynamic range between 50 and 251 was selected and it was suitable to clearly observe the evolution of the current inside the ambient fluid. For the selected dynamic range the maximum Rhodamine concentration is 5.765g/l.

3.2 Double calibration

Double calibration was adopted to analyze the two different flows. The first calibration was used to capture the surface gravity current while the second was conducted for the infiltration and the groundwater flow. Once the camera parameters, i.e. aperture of the lens and shutter speed, were set, it was possible to proceed with the fluid calibration shown in Figure 5, while the porous medium calibration is displayed in Figure 6.

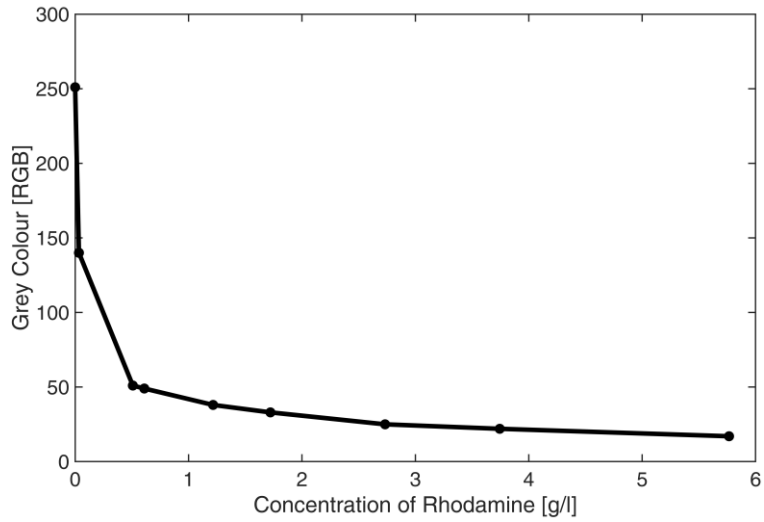


Figure 4. Gray scales versus increasing Rhodamine concentration

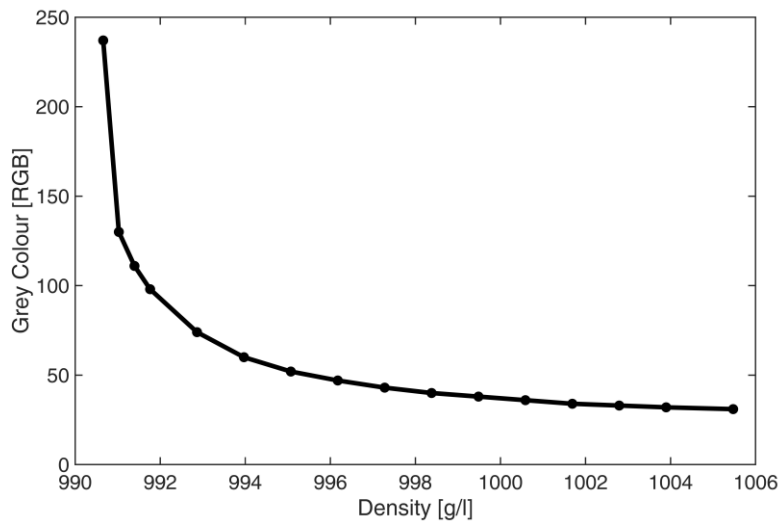


Figure 5. Gray scales versus density for water calibration

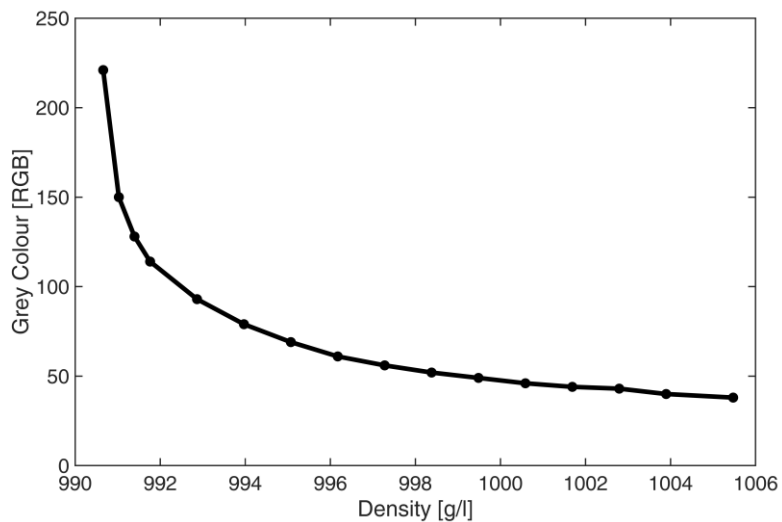


Figure 6. Gray scales versus density for beads calibration

3.3 Calibration curves

Each pixel is attributed a gray level as an average of the gray levels of the surrounding pixels. It allows to consider any light change by the camera and improves the accuracy of the calibration. In the present experiments there were two main phenomena affecting the quality of measurements. The first one involves the gravity current flow itself, which runs along the top of the porous bed. The second one involves the porous layer in horizontal and vertical directions. The light, generated by the LED panel, crosses the channel glass and changes in intensity and direction according to the material inside the channel. The top part was composed of water and alcohol, the porous bed is composed of spheres and the light is affected by the shape of the spheres, causing diffraction. The dynamic range in the present experiments consists in analyzing each pixel, i.e. the pixel (i, j), as an average of 5 x 5 surrounding pixels.

An area of 0.6 m x 0.40 m in the final part of the channel was used for the calibration. A porous bed layer, with a height of 0.1 m, was positioned in the calibration section and filled with water till to reach a water depth of 0.1 m above the porous bed. The calibration process was done twice, once for the water and the second one for the beads. Between these two calibrations, the aperture of the lens and the exposure time of the camera were modified. The calibration consisted of removing water from the tank and adding the denser fluid with Rhodamine in small quantities initially, then by gradually increasing until the last step, where it was required to remove the water and the spheres. Consequently, it was necessary to clean the channel and refill the path with the beads, but at this time, instead of water, the calibration section was filled only by dense fluid with Rhodamine in order to get the maximum concentration, i.e. the darkest color. Before the acquisition of the images for the calibration, it was crucial to take pictures with the checkerboard calibration pattern in order to rectify the images and eliminate any distortion.

It was possible to plot the calibration curve with the grey levels, corresponding to the 16 pictures taken with the water versus the density (g/l). For the beads, additional calculations were needed. Since the light passing through the beads was not uniform, it was crucial to have an average of the gray scales. Then four pictures were taken for each step, i.e. for each density, and after each picture the porous bed was mixed in order to change the distribution of the beads inside the layer and consequently change the gray scale distribution. After averaging the four images, the gray scale for each density was defined and a calibration curve with the grey levels versus density could be obtained for the beads.

Figure 7, relating the density and the grey scale, shows the calibration points for each step. The points vary between a gray scale of 250 and a gray scale of 50, with a range having more than 200 gray scales. The points of grey level versus density were fitted by a curve, containing 3 parameters and it is illustrated below:

$$Gr = a \cdot c^b + m \quad [1]$$

where Gr is the gray level, c is the concentration [g/l], and a , b , and m are the parameters. One example of fitting for one pixel is shown in Figure 7.

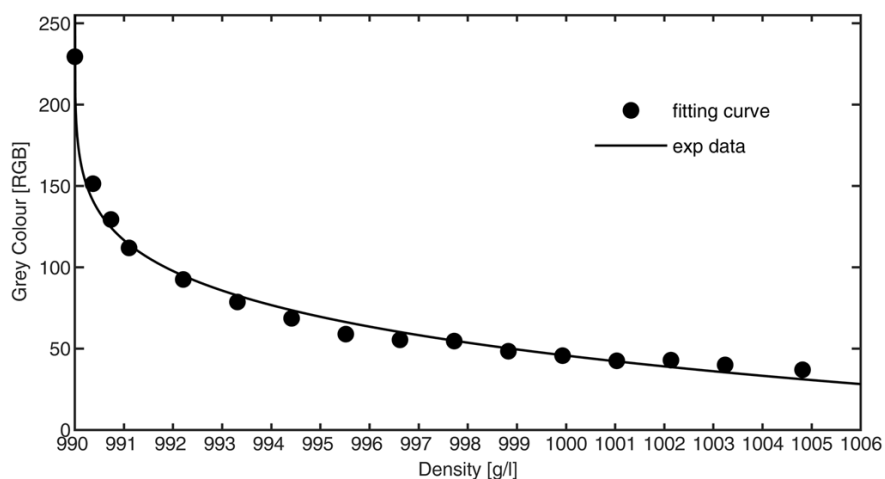


Figure 7. Calibration points with the fitted calibration curve

3.4 Image subtraction

The image subtraction is a process used to remove the optical noise within an image by subtracting the reference image to each frame. After the image subtraction, it was possible to fix the wide variation of grey

scales which makes difficult the detection of the flow inside the media. This subtraction leads to an inversion of the relationship between the grey levels and the concentration.

$$Gl(c) = a \cdot c^b + m \quad [2]$$

$$Im(i, j) = 255 \quad [3]$$

$$IGl = Im(i, j) - Gl(c) \quad [4]$$

$$IGl = Im(i, j) - a \cdot c^b + m \quad [5]$$

$$IGl = -a \cdot c^b + [Im(i, j) - m] \quad [6]$$

where Gl is the grey level, IGl is the inverse grey level, Im is the reference image, a , b , and m are the parameters, c is the concentration [g/l], and i, j are the pixel indexes. Figure 8 shows the image subtraction used to define the porous media flow and the gravity current flow.

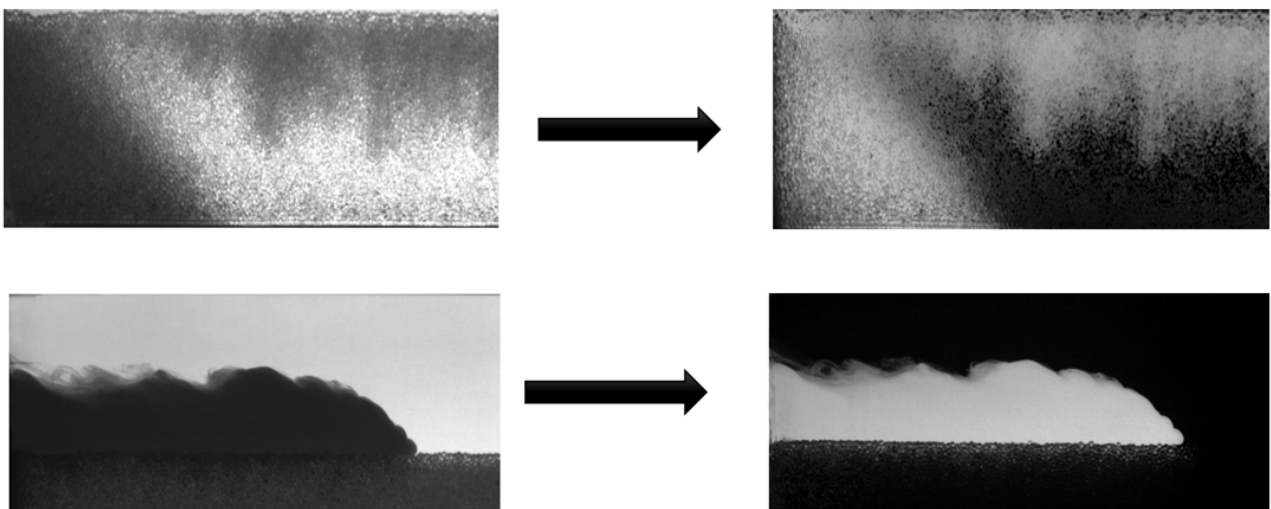


Figure 8. Pictures before and after image subtraction for: porous media (top) and water (bottom).

4 EXPERIMENTAL RESULTS

4.1 Surface gravity current

Figure 9 shows the dimensionless density fields, evaluated by image analysis, for a gravity current propagating over a smooth impermeable bed at different times. The dimensionless density ρ^* is defined as:

$$\rho^*(z, x, t) = \frac{\rho(z, x, t) - \rho_2}{\rho_1 - \rho_2} \quad [7]$$

where ρ_1 is the initial density of the salty lock fluid and ρ_2 is the ambient fluid density. Isolines of Figure 9 are plotted for 2, 10, 30, 35, 39, 47 [%].

Figure 10 shows the dimensionless density fields, evaluated by image analysis, for a gravity current propagating over unimodal porous bed at different times. Isolines of Figure 10 are plotted for 2, 10, 30, 35, 39, 47 [%].

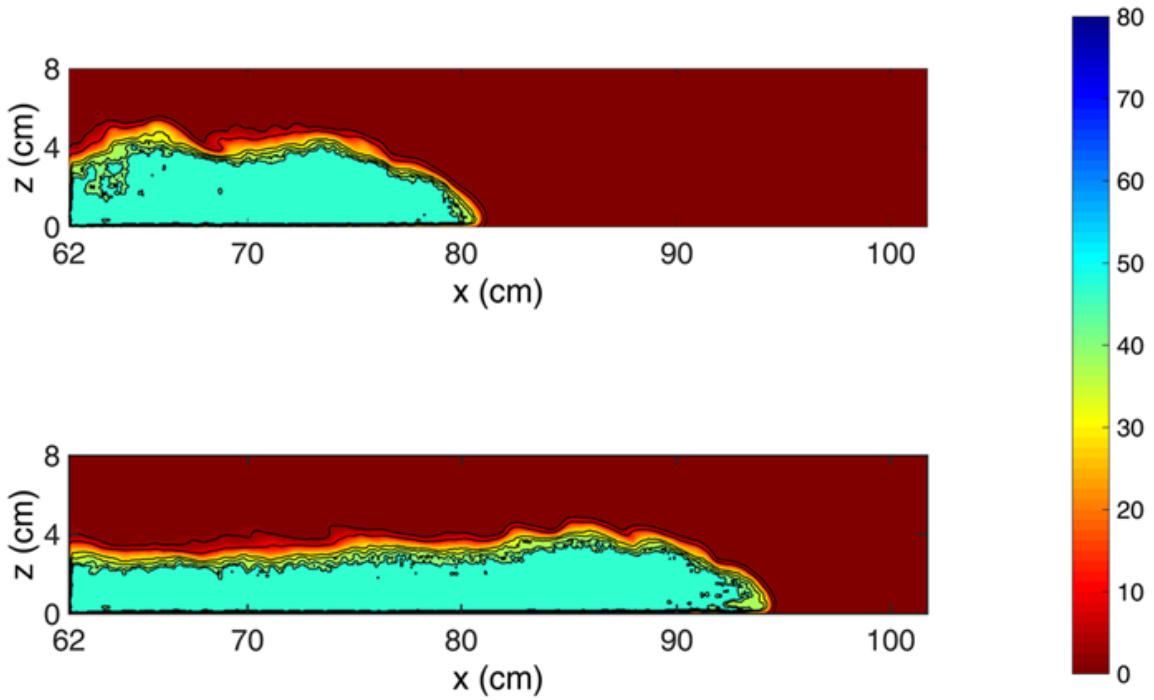


Figure 9. Colormaps of the dimensionless density field of a gravity current with $h_0 = 10$ cm propagating over smooth bed in the second measuring area at different times, i.e. $t = 12,5$ s and $t = 15,5$ s (from top to bottom).

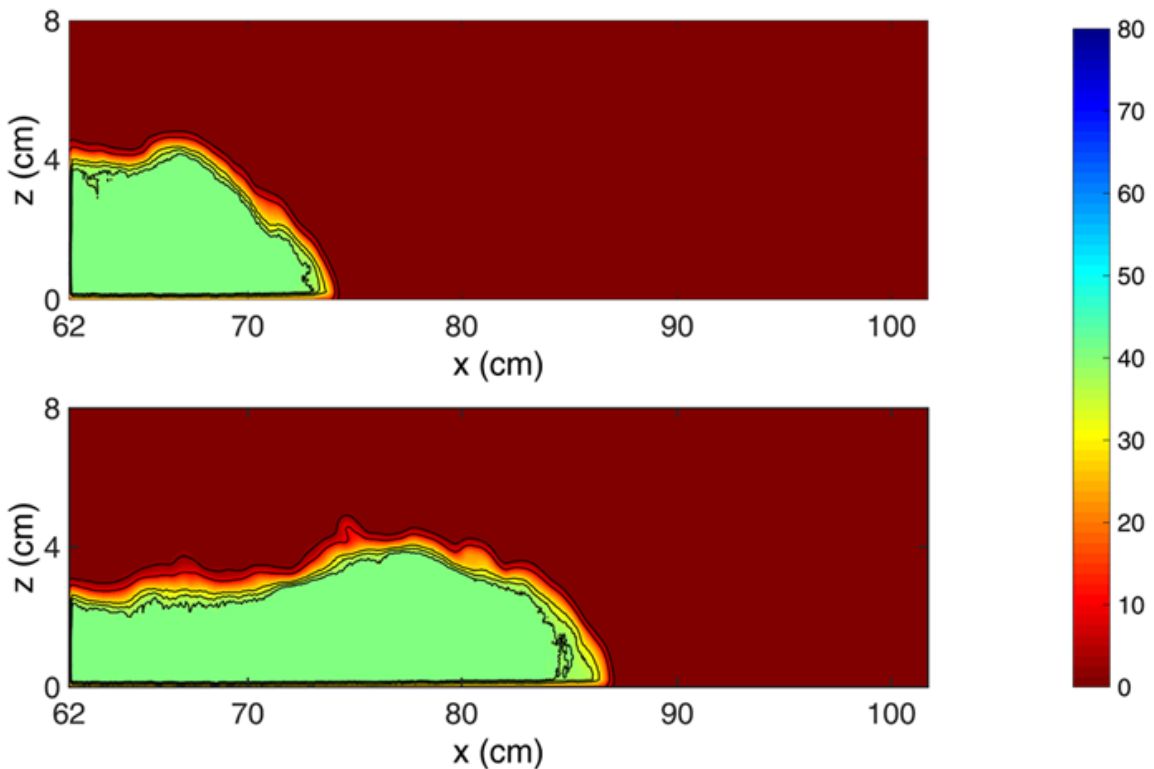


Figure 10. Colormaps of the dimensionless density field of a gravity current with $h_0 = 10$ cm propagating over unimodal porous bed in the second measuring area at different times, i.e. $t = 12,5$ s and $t = 15,5$ s (from top to bottom).

4.2 Infiltration and ground water flow

Figure 11 shows for the first measuring area and a unimodal porous bed the infiltration producing a fingering pattern and the propagation of the ground flow, i.e. a gravity current flowing within the porous bed, at different times. The lines plotted on the colour maps represent the isolines for 2, 5, 10, 30, 35, 39, 45, 60, 70 [%]. As time advances, a ground water flow with a sharp triangular front slowly propagates in the same direction of the

top gravity current flow. At the same time, due to the presence of a gravity current flowing above the porous bed, an infiltration flow develops at the top of the porous bed and propagates along the vertical direction. The infiltration develops a fingering instability.

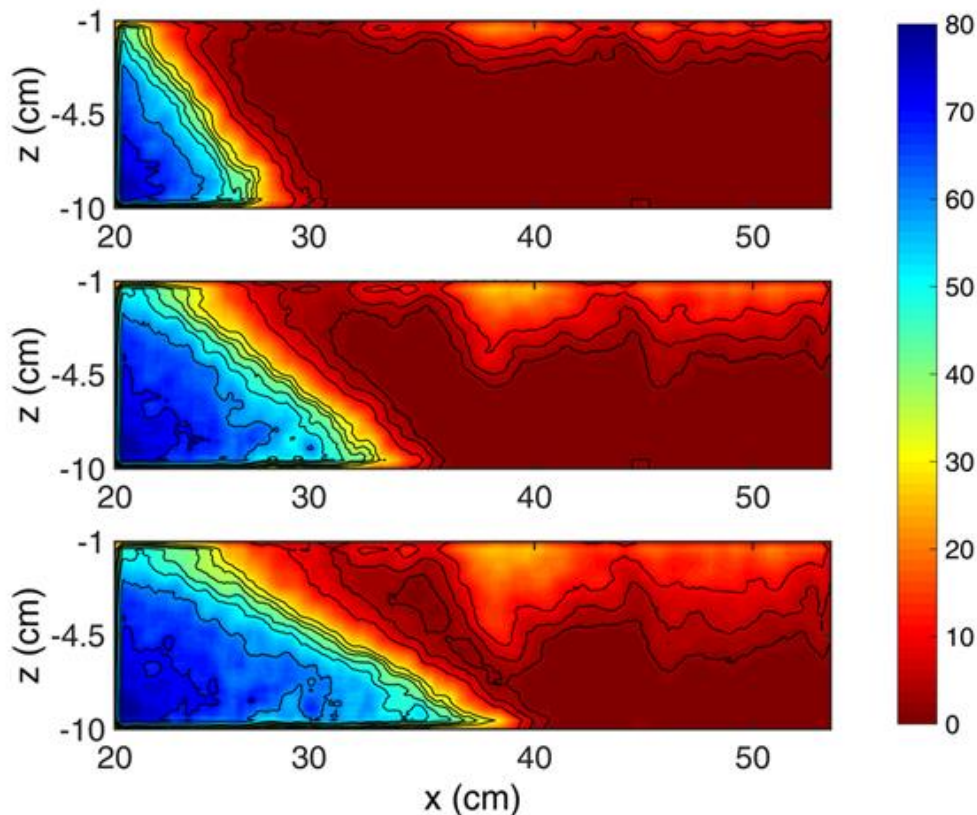


Figure 11. Infiltration analyzed by fingering and ground flow, i.e. gravity current flowing within the porous bed for different times $t = 60$ s, $t = 120$ s, $t = 180$ s (from top to bottom).

5 CONCLUSIONS

Important advances have been achieved in the characterization of the boundary-constricted motion of fluids with different density and viscosity with unstable stratifications in idealised geometries, namely Helle-Shaw cells. Advances in the particular case of granular media require more realistic geometries and visualization techniques. This work was a step in this direction, instabilization and propagation of plumes or fingers was analysed directly in a 3D granular medium with no important compromises or need for analogies.

Gravity currents propagating over and within a porous layer are investigated by laboratory experiments. Gravity currents are produced by the lock-release technique and full depth experiments are performed. The initial water depth and the bed composition were varied and unimodal and bi-modal porous beds were used. A camera was used to record the experiments both in a top domain, i.e. gravity current, and in a bottom one, ground flow and infiltration. An image analysis technique is applied for the evaluation of the instantaneous density fields and the different steps of the developed technique, i.e. gray scale calibration, double calibration, dynamic range and image subtraction, are discussed. The double image calibration was needed due to the large optical difference between the images captured in the top and bottom domains.

Preliminary results of the non-intrusive density measurements show a top gravity current propagating to the left of the tank and with a well defined head followed by a tail. In the bottom domain, a ground salty flow propagates in the same direction of the top flow, but with a slower velocity. The bottom gravity current has a sharp triangular front differing from the head of the top gravity current. In addition, the top gravity current causes infiltration in the porous layer and a fingering instability occurs. The preliminary results of this study reveal that the scales of plume growth may be different from those obtained from Helle-Shaw analogues. This finding may have an important impact in the communities involved in three-phase flow phenomena in the oil industry or in environmental flows such as wastewater through macrophyte beds. Future developments should see increasing amelioration of experimental optical and image analysis techniques to deal with true 3D flows in granular media.

ACKNOWLEDGEMENTS

This work was partially funded by national funds through Portuguese Foundation for Science and Technology (FCT) project Wintherface, PTDC/CTA-OHR/30561/2017.

REFERENCES

- Bhaganagar, K. (2014). Direct numerical simulation of lock-exchange density currents over the rough wall in slumping phase. *Journal of Hydraulic Research*, 52 (3), 386-398.
- Dai, A. (2013). Experiments on gravity currents propagating on different bottom slopes. *Journal of Fluid Mechanics*, 731, 117-141.
- Dai, A. and Huang, Y. (2016). High-resolution simulations of non-boussinesq downslope gravity currents in the acceleration phase. *Physics. Fluids*, 28(2), 026602.
- Golding, M.J., Huppert, H.E., & Neufeld, J.A. (2017). Two-phase gravity currents resulting from the release of a fixed volume of fluid in a porous medium. *Journal of Fluid Mechanics*, 832, 550-577.
- Hacker, J., Linden, P.F., & Dalziel, S.B. (1996). Mixing in lock-release gravity currents. *Dynamics of Atmospheres and Oceans*, 24, 183-195.
- Huppert, H.E. & Woods, A.W. (1995). Gravity-driven flows in porous layers. *Journal of Fluid Mechanics*, 292, 55-69.
- Inghilesi, R., Adduce, C., Lombardi, V., Roman, F. and Armenio, V. (2018). Axisymmetric three-dimensional gravity currents generated by lock exchange. *Journal of Fluid Mechanics*, 851, 507-544.
- La Rocca M., Prestininzi P., Adduce C., Sciortino G. and Hinkelmann R. (2013). Lattice Boltzmann simulation of 3D gravity currents around obstacles. *International Journal of Offshore and Polar Engineering*, 23(3), 178-185.
- Lombardi, V., Adduce, C. and La Rocca, M. (2018). Unconfined lock-exchange gravity currents with variable lock width: laboratory experiments and shallow-water simulations. *Journal of Hydraulic Research*, 1-13.
- Marino, B.M., Thomas, L.P., & Linden, P.F. (2005). The front condition for gravity currents. *Journal of Fluid Mechanics*, 536, 49-78.
- Nogueira, H. I. S., Adduce, C., Alves, E. and Franca, M. J. (2013). Analysis of lock-exchange gravity currents over smooth and rough beds. *Journal of Hydraulic Research*, 51(4), 417-431.
- Nogueira, H.I.S., Adduce, C., Alves, E. & Franca, M.J. (2014). Dynamics of the head of gravity currents. *Environmental Fluid Mechanics*, 14(2), 519-540.
- Ooi, S. K., Constantinescu, G. and Weber, L. (2009). Numerical simulations of lock-exchange compositional gravity current. *Journal of Fluid Mechanics*, 635, 361-388.
- Ottolenghi, L., Adduce, C., Roman, F. and Armenio, V. (2017a). Analysis of the flow in gravity currents propagating up a slope. *Ocean Modelling*, 115, 1-13.
- Ottolenghi, L., Cenedese, C. and Adduce, C. (2017b). Entrainment in a dense current flowing down a rough sloping bottom in a rotating fluid. *J. Physical Oceanography*, 47(3), 485-498.
- Ottolenghi, L., Prestininzi, P., Montessori, A., Adduce, C. and La Rocca, M. (2018). Lattice Boltzmann simulations of gravity currents. *European Journal of Mechanics-B/Fluids*, 67, 125-136.
- Ozgokmen, T.M., & Fischer, P.F. (2008). On the role of bottom roughness in overflows. *Ocean Modelling*, 20 (9), 336 - 361.
- Woods, A.W., & Mason, R. (2000). The dynamics of two-layer gravity-driven flows in permeable rock. *Journal of Fluid Mechanics*, 421, 83-114.
- Zordan, J., Juez, C., Schleiss, A. J. and Franca, M. J. (2018). Entrainment, transport and deposition of sediment by saline gravity currents. *Advances in Water Resources*, 115, 17-32.